Amino Acids (2014) 46:2137–2154
DOI 10.1007/s00726-014-1761-8

ORIGINAL ARTICLE

Cell specificity and molecular mechanism of antibacterial and antitumor activities of carboxyl-terminal RWL-tagged antimicrobial peptides

N. Dong · X. Zhu · Y. F. Lv · Q. Q. Ma · J. G. Jiang · A. S. Shan

Received: 18 March 2014 / Accepted: 7 May 2014 / Published online: 29 May 2014

Abstract Antimicrobial peptides (AMPs) constitute a diverse class of naturally occurring or synthetic antimicrobial molecules that have potential for use in the treatment of drug-resistant infections. Several undesirable properties of AMPs, however, may ultimately hinder their development as antimicrobial agents. Thus, new synthetic strategies, including primarily the de novo design of AMPs, urgently need to be developed. In this study, a series of peptides, H-(RWL)$_n$ (n = 1, 2, 3, 4, or 5), were designed. H represents GLRPKYS from the C-terminal sequence of AvBD-4. Our results showed that these RWL-tagged peptides can kill not only bacteria but also human hepatocellular carcinoma HepG2 cells. However, the peptide tagged with two repeats of RWL (GW13) showed less affinity to human embryonic lung fibroblast MRC-5 cells or human red blood cells (hRBCs) than HepG2 cells. These results demonstrated that GW13, with high amphiphilicity, exerted great selectivity toward bacteria and cancer cells, sparing host mammalian cells. The mechanism of action against bacteria was elucidated through combined studies of scanning electron microscopy (SEM) and fluorescence assays, showing that the peptide possessed membrane-lytic activities against microbial cells. The fluorescence assays illustrated that GW13 induced apoptosis in HepG2 cells. The cell morphology of HepG2 cells, observed by SEM, further illustrated that GW13 causes cell death by damaging the cell membrane. Our results indicate that GW13 has considerable potential for future development as an antimicrobial and antitumor agent.

Keywords Antimicrobial peptides · Cell specificity · Membrane permeability · Hemolysis · Apoptosis

Abbreviations

AMP	Antimicrobial peptide
MIC	Minimum inhibitory concentration
MHC	Minimal hemolytic concentration
CD	Circular dichroism
SDS	Sodium dodecyl sulfate
PC	Phosphatidylcholine
PE	Phosphatidylethanolamine
PG	Phosphatidylglycerol
MH	Mueller–Hinton
PI	Propidium iodide
CCCP	Carbonyl cyanide m-chlorophenylhydrazone

N. Dong · X. Zhu · Y. F. Lv · Q. Q. Ma · A. S. Shan (✉)
Laboratory of Molecular Nutrition and Immunity, Institute of Animal Nutrition, Northeast Agricultural University, 59 Mucai Street, Harbin 150030, China
e-mail: asshan@neau.edu.cn

N. Dong
e-mail: ndong@neau.edu.cn

J. G. Jiang
State Key Laboratory of Electroanalytical Chemistry, Changchun Institute of Applied Chemistry, Chinese Academy of Sciences, 5625 Ren Min Street, Changchun 130022, China

Introduction

Antimicrobial peptides (AMPs) secreted by the innate immune system of various organisms such as vertebrates, insects, and even bacteria, represent the first line of defense against pathogen challenges (Zasloff 2002; Selsted and Ouellette 2005). AMPs have distinctive modes of action; it is widely recognized that AMPs are membrane-lytic molecules, distinguishing them from pharmaceutical

antibiotics and suggesting that AMPs can potentially be superior to traditional antibiotics in overcoming multidrug resistance. Indeed, data from both the laboratory and the clinic in the last decade indicate that AMPs are a promising solution for combatting multidrug-resistant microbial infections (Hancock and Sahl 2006; Wang et al. 2011). Moreover, AMPs are being extensively evaluated for use in bioengineering and biomedical applications (Wiradharma et al. 2011a, b; Chen et al. 2012). However, the road leading to widespread clinical applications of AMP is imperiled; issues such as toxicity to human cells, high production cost, and stability against proteases will likely hinder the further development of natural peptides as future antibiotic drugs (Bell 2011). Therefore, in order to solve the above problems, research has increasingly focused on the empirical optimization of these peptides by chemical modifications, such as glycosylation, fluorination, cyclization, and the introduction of amino acid point mutations (Hu et al. 2009; Zheng et al. 2007; Subbalakshmi et al. 2000; Guillen Schlippe et al. 2012).

AMPs approach the surface of bacteria and lyse their cell membranes, requiring both cationic and hydrophobic amino acids to achieve this activity (Wieprecht et al. 1999; Ladokhin and White 1999). The side chains Arginine (R), Lysine (K), and Histidine (H), with cationic charges, favor AMP binding at the negatively charged membrane surfaces of target bacterial cells via electrostatic attraction (Ladokhin and White 1999). Bulky, nonpolar side chains, such as Tryptophan (W), Leucine (L) and Proline (P), occur frequently in AMPs, presumably providing lipophilic anchors that ultimately cause membrane disruption (Tam et al. 2002). Recently, new synthetic strategies utilizing the de novo design of AMPs were adopted, and one type of AMP with a specific amino acid residue stacking arrangement displayed great antibacterial potential and cell selectivity (Wiradharma et al. 2011b; Dong et al. 2012c; Deslouches et al. 2005). Wiradharma et al. synthesized a series of cationic amphiphilic α-helical peptides of 2–4 repeating units, composed of hydrophobic and cationic residues, which displayed excellent antibacterial activity against the frequently encountered gram-positive bacteria or yeast-induced infections (Wiradharma et al. 2011b). We previously designed and synthesized a series of Arg- and Val-rich β-hairpin-like peptides, Ac–C$(VR)_n^D$PG $(RV)_n$C–NH_2 (n = 1, 2, 3, 4, or 5), and our results showed that the 16-mer peptide (VR3) with seven amino acids in each strand showed the highest therapeutic index (Dong et al. 2012c). Deslouches et al. designed a series of multimers from a 12-residue lytic base unit (LBU) composed only of Arg and Val, which were aligned to form idealized amphipathic helices. Their results showed that two-LBU peptides (24-residues) achieved optimal activity against *P. aeruginosa* (Deslouches et al. 2005). These observations indicated that repetition of simple amino acid sequences including hydrophilic and hydrophobic residues may be a feasible, effective strategy to discover new AMPs with greater selectivity, while circumventing inherent toxicity and stability issues.

In addition to AMPs having bactericidal activities, the potential for killing tumor cells has been investigated. Several AMPs have been reported to show potency in killing tumor cells (Standley et al. 2010; Hu et al. 2011). It remains to be determined whether AMPs will succeed as antibiotic substitutes or novel anticancer agents and whether the AMP anticancer activity differs in its mechanism of activity from that for antibacterial activity.

In the past few years, several AMPs have been evaluated in preclinical and clinical trials (Rubinchik et al. 2009; Yeung et al. 2011). However, there is an argument increasingly stated that clinical use of AMPs with significant sequence similarity to human AMPs would inevitably compromise innate defenses, possibly posing a threat to public health (Bell and Gouyon 2003). Reducing homology to human AMPs and combining simple amino acid repeated sequences will likely avoid causing these problems. Most recently, we reported that the truncation of the C-terminal region of AvBD-4 (RYHMQCGYRGTFCTP GKCPYGNAYLGLCRPKYSCCRWL), chicken β-defensin isolated from chicken epithelial tissues, retained the antimicrobial activity and decreased its cytotoxicity (Dong et al. 2012a, b); the shortest peptide GL13 maintained antimicrobial activity. In this study, a series of peptides, H-$(RWL)_n$ (n = 1, 2, 3, 4, or 5), were designed. H represents GLRPKYS, truncated from the 13-mer C-terminal sequence of AvBD-4, with the 3 cysteines deleted. H-$(RWL)_n$ includes 3-residue RWL repeats. The RWL sequence is the C-terminal trimer of AvBD-4. The quantitative structure–activity relationships of R, W and L motifs have been investigated individually; for example, the hydrophilic and cationic amino acid Arg is thought to mediate peptide interactions with negatively charged membranes of bacteria. The antimicrobial activity of peptides containing Arg is greater than that of peptides containing Lys (Shafer et al. 1996). In addition, the side chain of W interacts more efficiently with membrane surfaces compared with other nonpolar side chains, making peptides including W more potent AMPs than those containing other hydrophobic amino acids, such as F or L (Dathe et al. 2004; Subbalakshmi et al. 2000). Leu-rich AMPs have potent antibacterial activity equivalent to that of melittin (Beven et al. 2003). We speculate that the number of 3-residue RWL repeats will affect the antimicrobial activity and toxic effects to normal somatic cells, and an optimal length for maximal biological activity is likely to exist. The peptides were first characterized for their secondary conformation in both solution and a simulated

membrane environment by circular dichroism (CD). The antimicrobial properties of the peptides were evaluated using MIC measurement against a broad selection of practical and potentially threatening microbes such as *E. coli*, *S. Pullorum, S.* Typhimurium, *B. yocyaneum* (gram negative), *S. aureus, S. epidermidis, S. faecalis,* and *B. subtilis* (gram positive). To investigate the potential membrane-destruction mechanisms of the peptides, the tryptophan fluorescence spectra of tryptophan-containing peptides, flow cytometric analysis, confocal laser-scanning microscopy, and SEM micrographs were employed. In addition, the mode of action of these peptides against tumor cells was determined using annexin-V-FITC/PI staining, Hoechst 33258/PI staining, a mitochondrial membrane potential assay, and scanning electron microscopy, which together could differentiate whether the mechanisms of toxicity were related to the cell membrane or to the intracellular machinery.

Materials and methods

Materials

Peptides and relevant reagents of molecular characterization were obtained from GL Biochem (Shanghai, China). Sodium dodecyl sulfate (SDS) micelles was obtained from Amresco (USA) and used upon dilution to 30 mM in DI water. Ethanol (analytical grade, 99 %), acetone (analytical grade, 99 %), *tert*-butanol (analytical grade, 99 %) and glutaraldehyde (synthetic grade, 50 % in H_2O), and small unilamellar vesicles (SUVs) including egg yolk L-α-phosphatidylcholine (PC), egg yolk L-α-phosphatidyl-DL-glycerol (PG) and egg yolk L-α-phosphatidylethanolamine (PE), and cholesterol, acrylamide, propidium iodide (PI), carbonyl cyanide *m*-chlorophenylhydrazone (CCCP) and Hoechst 33258/PI were obtained from Sigma-Aldrich Corporation (St. Louis, MO, USA). The cationic dye JC-1 was purchased from Beyotime (Shanghai, China) and the Annexin-V-FITC/PI Apoptosis Detection Kit was obtained from Biosea (Beijing, China).

Tested strains *Escherichia coli* ATCC 25922, *Salmonella enterica* serovar Typhimurium C77-31, *Salmonella* Typhimurium C79-13, *Bacterium pyocyaneum* ATCC 27853, *Staphylococcus aureus* ATCC 29213, *Staphylococcus epidermidis* ATCC 12228, *Streptococcus faecalis* ATCC 29212, and *Bacillus subtilis* CMCC 63501 were obtained from the College of Veterinary Medicine, Northeast Agricultural University (Harbin, China). The bacteria were incubated in Mueller–Hinton Broth (MHB) media (beef infusion solids, 5 g/l, casein hydrolysate, 17.5 g/l, soluble starch 1.5 g/l, pH 7.0 ± 0.2), purchased from AoBoX (Shanghai, China). Red blood cells (RBCs) used in the experiments were extracted from healthy blood donors. Human embryonic lung fibroblast MRC-5 cells were purchased from the Institute of Biological and Cell Biology, SIBS, CAS. Human hepatocellular carcinoma HepG2 cells were obtained from the College of Life Science, Northeast Agricultural University (Harbin, China). MTT (3-(4,5-Dimethylthiazol-2-yl)-2,5-diphenyltetrazolium bromide) was purchased from Sigma-Aldrich Corporation (St. Louis, MO, USA), and DMEM supplemented with L-glutamine and 10 % fetal calf serum was obtained from Invitrogen Corporation (USA).

Peptide synthesis

The peptides were synthesized by GL Biochem Corporation (Shanghai, China) by solid-phase methods using N-(9-fluorenyl) methoxycarbonyl (Fmoc) chemistry. The C-terminus was amide protected. Each peptide's identity was further confirmed via matrix-assisted laser desorption/ionization time-of-flight mass spectroscopy (MALDI-TOF MS, Linear Scientific Inc., USA). The purity of the peptides was determined to be greater than 95 % by analytical reverse phase (RP)-HPLC. The amino acid sequence and molecular weight of the peptides used in this study are shown in Table 1. Peptides were dissolved in pure water at a concentration of 2.56 mM, and the peptide solutions were stored at −20 °C before subsequent antibacterial, antitumor, and other structural assessments.

Computational modeling and sequence analysis of peptides

The structures of the peptide models were built using ChemOffice Desktop 2004 for Windows (CambridgeSoft Corporation, MA, USA). The structures of linear peptides were generated, and the energies were minimized using Chem3D with the molecular mechanics method (MM2) (Burkert and Allinger 1982). The sequences of the peptides were initially added using standard ChemDraw Ultra, after which the N- and C-termini of the peptide groups were acylated and amidated, respectively. Energy minimizations were run for all of the peptides using the Chem3D MM2 method. Finally, optimized peptides were imported into the Jmol program for visualization and figure generation (http://www.jmol.org/). The mean hydrophobicity and relative hydrophobic moment were calculated online using the *Kyte–Doolittle* scale (http://www.bbcm.univ.trieste.it/~tossi/HydroCalc/HydroMCalc.html).

CD analysis

To investigate the secondary structure of the peptides in different environments, CD spectra were measured under

Table 1 Amino acid sequence, molecular weight, net charge, and hydrophobicity value of the peptides used in this study

Peptide	Sequence	Mw (Da)[a]		H[b]	u[c]	Net charge
		Calculated	Observed			
GW10	GLRPKYS$(RWL)_1$-NH_2	1,274.52	1,274.55	−1.03	0.87	+4
GW13	GLRPKYS$(RWL)_2$-NH_2	1,730.08	1,730.11	−0.91	1.25	+5
GW16	GLRPKYS$(RWL)_3$-NH_2	2,185.64	2,185.68	−0.84	1.24	+6
GW19	GLRPKYS$(RWL)_4$-NH_2	2,641.20	2,641.24	−0.79	0.96	+7
GW22	GLRPKYS$(RWL)_5$-NH_2	3,096.76	3,096.80	−0.75	0.54	+8
IN13	ILPWKWPWWPWRR-NH_2	1,906.29	1,906.33	−1.06	0.19	+4

[a] *Mw* molecular weight in Daltons

[b] *H* the hydrophobicity per residue of peptides calculated by the methods of *Kyte and Doolittle*

[c] *u* mean hydrophobicity moment of peptides calculated by the methods of *Kyte and Doolittle*

inert conditions of 10 mM sodium phosphate buffer (pH 7.4) and 30 mM SDS micelles. The CD spectra of peptides were measured at 25 °C with a J-820 spectropolarimeter (Jasco, Tokyo, Japan) equipped with a rectangular quartz cell with a path length of 0.1 cm. Spectra were recorded at a scanning speed of 10 nm/min from 190 to 250 nm. An average of five to eight scans was collected for each peptide. The final concentration of peptides was 150 μM.

The acquired CD signal spectra were then converted to mean residue ellipticity using the following equation:

$$\theta_{\mathrm{M}} = (1,000 \cdot \theta_{\mathrm{obs}})/n \cdot c \cdot l$$

where θ_{M} is residue ellipticity (deg cm^2 dmol^{-1}), θ_{obs} is the observed ellipticity corrected for the buffer at a given wavelength (mdeg), n is the number of amino acids, c is peptide concentration (mM), and l is the path length (cm).

Antimicrobial assays

The minimum inhibitory concentrations (MICs) of the peptides were measured using a modified version of the Clinical Laboratory and Standards Institute broth microdilution method to determine the in vitro antimicrobial activities of the peptides (Yang et al. 2001). Bacteria were grown overnight at 37 °C to mid-log phase and then diluted in MHB to give a final concentration ranging from 2×10^5 to 7×10^5 CFU/ml. Peptides were dissolved and diluted in 0.01 % acetic acid and 0.2 % bovine serum albumin (BSA, Sigma). The bacterial aliquots of 100 μl were incubated for 18–24 h at 37 °C with 100 μl of peptide in MHB. The tests were performed in triplicate. The MICs were calculated as the lowest concentration of peptide that prevented visible turbidity.

Quantification of hemolytic activity

Fresh human red blood cells (hRBCs) were collected and then centrifuged at 1,000×*g* for 5 min at 4 °C. The erythrocytes obtained were washed three times with phosphate-buffered saline (PBS) buffer (pH 7.2) and resuspended in PBS to attain a dilution of ~1 % (v/v) of the erythrocytes. A 100-μl hRBCs solution was incubated with 100 μl of the respective peptide dissolved in PBS for 1 h at 37 °C. Intact erythrocytes were centrifuged at 1,000×*g* for 5 min at 4 °C, and the supernatant was transferred to a 96-well microtiter plate. The release of hemoglobin was monitored by measuring the absorbance at 570 nm (OD_{570}). As negative and positive controls, hRBCs in PBS and 0.1 % Triton X-100 were used, respectively. Minimum hemolytic concentrations (MHCs) are defined as the peptide concentrations resulting in 10 % hemolysis.

Tryptophan fluorescence and quenching

Small unilamellar vesicles (SUVs) were prepared for tryptophan fluorescence experiments as described previously (Lee et al. 2006). Following chloroform evaporation, the PE/PG (7:3, w/w) or PC/cholesterol (10:1, w/w) lipids were resuspended in 10 mM Tris–HCl buffer (10 mM Tris, pH 7.4, 150 mM NaCl, 0.1 mM EDTA) by vortexing. The lipid dispersions were sonicated in ice water for 20 min using an ultrasonic cleaner until the solutions clarified. Tryptophan fluorescence spectra were measured using an F-4500 fluorescence spectrophotometer (Hitachi, Japan). The procedure was performed for each peptide in 10 mM Tris–HCl buffer (pH 7.4) with 500 μM PE/PG or PC/cholesterol lipids. The peptide/lipid molar ratio was 1:50, and the peptide/liposome mixture was allowed to interact for 2 min at 25 °C. An excitation wavelength of 280 nm was used, and emission was scanned at wavelengths ranging from 300 to 400 nm. The spectra were baseline-corrected by subtracting blank spectra of the corresponding solutions without the peptide. The quenching of fluorescence was accomplished using acrylamide. To reduce the absorbance of acrylamide, Trp was excited at 295 nm instead of 280 nm. The final concentration of acrylamide was brought to 0.4 M by titrating the 4 M stock solution

with liposomes at a lipid/peptide molar ratio of 50:1. The effects of the quenching reagent on peptide fluorescence intensities were assessed by the quenching constant (K_{SV}), which was estimated using the Stern–Volmer equation: $F_0/F = 1 + K_{SV}$ (Q), where F_0 and F are the fluorescence values of the peptide in the absence or the presence of acrylamide, respectively, K_{SV} represents the Stern–Volmer quenching constant, and Q represents the concentration of acrylamide.

FACScan analysis

E. coli was grown to log phase and harvested. The peptides were added and incubated for 30 min at 28 °C with constant shaking at 140 rpm. The cells were harvested by centrifugation, washed three times, and incubated with propidium iodide (PI, 10 μg/ml final concentration) at 4 °C for 30 min, followed by removal of the unbound dye by washing with an excess of PBS. Flow cytometry was performed using a FACScan instrument (Becton–Dickinson, San Jose, CA).

Confocal laser-scanning microscopy

E. coli cultures were grown to the mid-logarithmic phase. *E. coli* cells (10^7 CFU/ml) in 10 mM PBS, pH 7.4 were incubated with FITC-labeled peptides (1 × MIC; 2 × MIC; 5 × MIC) at 37 °C for 30 min. Next, the cells were washed with PBS and immobilized on a glass slide. Confocal fluorescence images were used to examine the interaction between FITC-labeled AMPs and cell walls with a Leica TCS SP1 microscope. The fluorescent images were obtained with a 488 nm band-pass filter for FITC excitation.

Field emission scanning electron microscopy (FE-SEM) analysis of bacterial cells

E. coli ATCC 25922 and *S. aureus* ATCC 29213 cells were cultured in MHB at 37 °C under constant shaking at 200 rpm overnight. Logarithmic phase bacteria were centrifuged at 5,000×*g* for 5 min, washed twice with 10 mM PBS, and resuspended. The concentration of bacterial suspension was adjusted to give an initial optical density (OD) reading of 0.1–0.2 at 600 nm wavelength. Peptide treatment of the bacterial cells was at 37 °C for 1 h at a concentration of 1 × MIC. Bacteria incubated with PBS served as the control. Following the incubation, the cells were mixed and centrifuged at 5,000×*g* for 5 min. The bacterial cells were then centrifuged and washed with PBS three times and fixed with 2.5 % (w/v) glutaraldehyde at 4 °C overnight, followed by washing with PBS twice. The bacterial pellets were dehydrated with a series of graded ethanol solutions (50, 70, 80, 90, 95 and 100 %). Upon dehydration, the dried bacterial cells were transferred to a mixture (v:v = 1:1) of alcohol and *tert*-butanol for 30 min, followed by pure *tert*-butanol for 1 h. The specimens were then dried using a critical point dryer. The dried bacterial specimens were coated and visualized under a field emission scanning electron microscope (Hitachi S-4800, Japan).

To examine the morphology of peptide-treated tumor cells, HepG2 cells were pre-seeded on coverslips at a density of 3×10^4 cells/ml for 24 h at 37 °C in a 5 % CO_2 atmosphere. The peptide solution was added to a final concentration of 32, 64, or 128 μM, and the cultures were incubated for an additional 24 h. The medium was then removed, and 1 ml of 4 % glutaraldehyde solution was added to each well for 1.5 h. The cells were washed in PBS (pH 7.2) three times, dehydrated in ethanol, and dried in a critical point dryer. The cells on coverslips were coated with gold and analyzed according to these methods.

Analysis of cell viability

Human embryonic lung fibroblast MRC-5 and human hepatocellular carcinoma HepG2 (1.0×10^4 cell/well) cells in DMEM supplemented with L-glutamine and 10 % fetal calf serum were placed into 96-well plates, then incubated under a fully humidified atmosphere of 95 % air and 5 % CO_2 at 37 °C overnight. The next day, the peptides were added to cell cultures at final concentrations of 1–128 μg/ml. After incubation for 24 h, the cell cultures were incubated with MTT (50 μl, 0.5 mg/ml) for 4 h at 37 °C. The cell cultures were centrifuged at 1,000×*g* for 5 min, and the supernatants were discarded. Subsequently, 150 μl of dimethyl sulfoxide was added to dissolve the formazan crystals formed. The OD was measured using a microplate reader (TECAN GENios F129004; TECAN, Austria) at 492 nm.

Annexin-V-FITC/PI double staining

Apoptosis of HepG2 cells was determined using the Annexin-V-FITC/PI Apoptosis Detection Kit. HepG2 cells (1×10^6 cells/well) were incubated in 6-well plates with peptides at 37 °C, while no peptide was added to the control wells. The cells were centrifuged at 1,000 rpm for 10 min at 4 °C three times, and the pelleted cells were then incubated in 200 μl of binding buffer. Ten microliters of Annexin-V-FITC was added to the solutions at 4 °C in the dark for 30 min, followed by an additional 300 μl binding buffer. Five microliters of PI was added 5 min prior to analysis of the cells by flow cytometry (Becton–Dickinson, San Jose, CA). The experiment was performed three times.

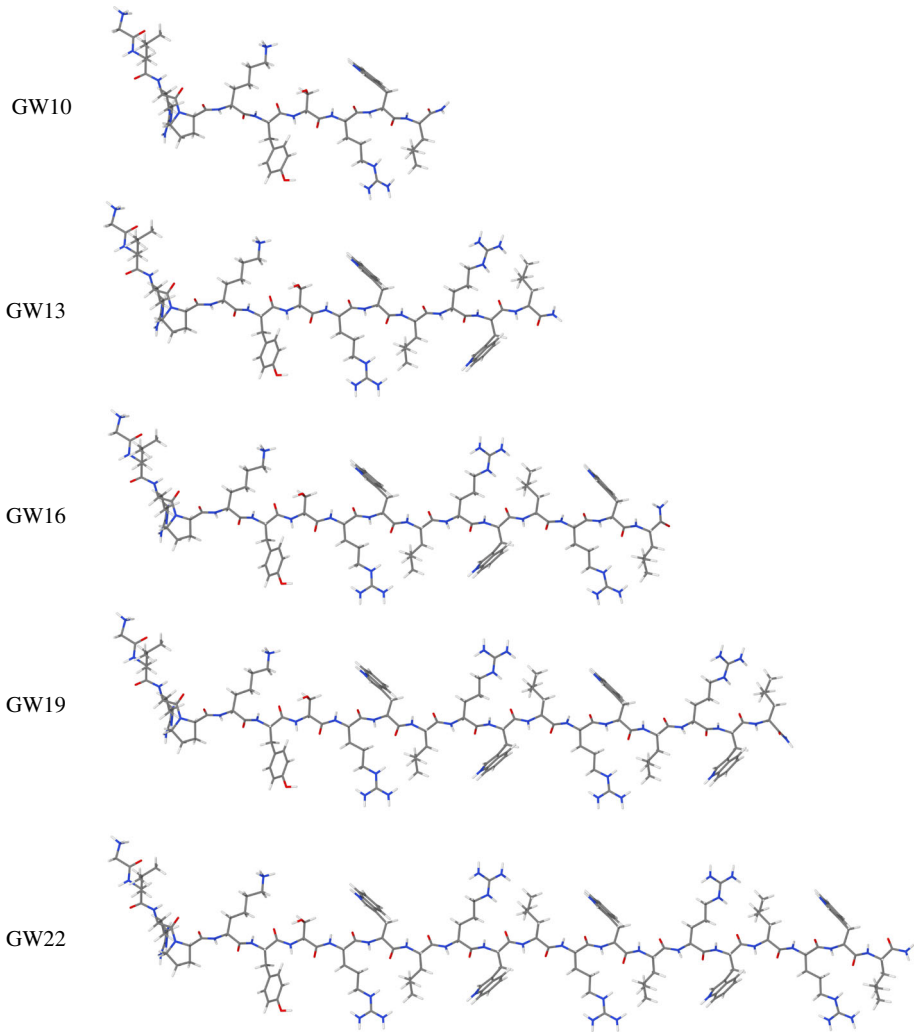

Fig. 1 Model structures of H-(RWL)$_n$ (n = 1, 2,3, 4, or 5). The structures of linear peptides were generated and the energies minimized using Chem3D and the molecular mechanics method (MM2). The peptides are displayed as *capsticks*, with carbon atoms in *gray*, nitrogen atoms in *blue*, and oxygen and hydrogen atoms in *red* and *white*, respectively (color figure online)

Hoechst 33258/PI double staining

The analysis of nuclear morphology was performed using a Hoechst 33258/PI double-staining assay. The peptide-treated cells were fixed with a 50 % solution of 3:1 methanol/acetic acid for 10 min. The fixed cells were stained with Hoechst 33258 at 1 μg/ml in the dark for 10 min at room temperature and then with PI at 1 μg/ml in the dark for 20 min at 4 °C. The cells were then washed three times with PBS, and the nuclear morphology was analyzed using a laser-scanning confocal microscope (LEICA, TCS, SPI). The experiment was performed three times.

Mitochondrial membrane potential assay

Mitochondrial membrane potential changes were assessed using the cationic dye JC-1 (5 μg/ml). Briefly, HepG2 cells (1×10^6 cells/well) were incubated with tested peptide or with no peptide addition as control. The cells were incubated with JC-1 staining solution (5 μg/ml) at 37 °C for 20 min and rinsed twice with PBS. Mitochondrial depolarization was indicated by an increase in the green/red fluorescence intensity ratio using a laser-scanning confocal microscope (LEICA, TCS, SPI). The experiment was performed three times.

Statistical analysis

Data were analyzed by ANOVA using SPSS 16.0 software. Quantitative data are presented as the mean ± standard deviation of the mean. Significant differences were identified at the value of <0.05 or <0.01.

Results

Molecular and secondary structures

The structure and molecular weight of the peptides were verified by MALDI-TOF MS. Table 1 summarizes the theoretically calculated and measured molecular weight of

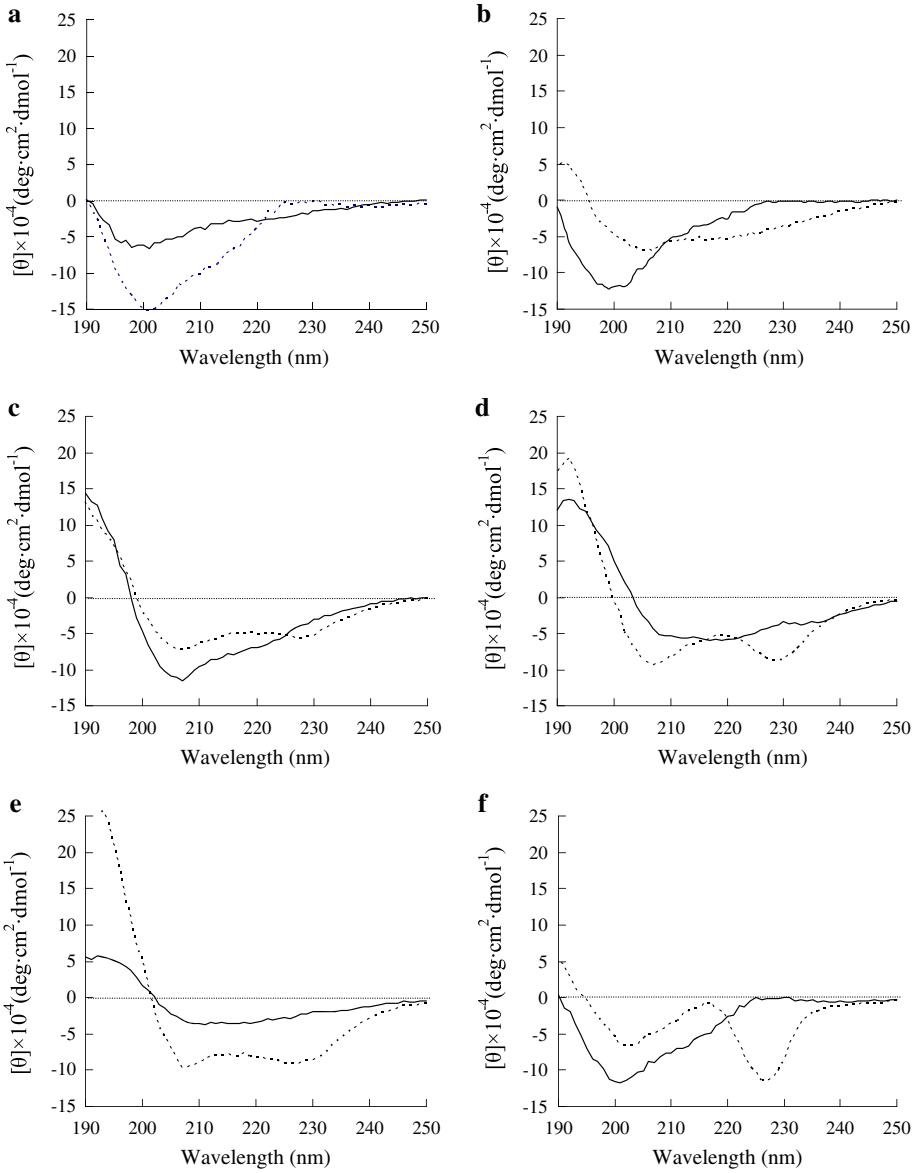

Fig. 2 CD spectra of GW10 (**a**), GW13 (**b**), GW16 (**c**), GW19 (**d**), GW22 (**e**), and IN13 (**f**). The peptides were dissolved in 10 mM PBS (pH 7.4) (*solid line*) and 30 mM SDS (*dotted line*), respectively. The mean residue ellipticity was plotted against wavelength. The values from three scans were averaged per sample, and the peptide concentrations were fixed at 150 μM

each peptide. All peptides had molecular weight values in agreement with their theoretical values, suggesting that the peptides were successfully synthesized. Computer modeling revealed that the clustering of RWL motifs within $(RWL)_n$ peptides resulted in outstretched spatial arrangements and surface areas (Fig. 1).

Circular dichroism was performed for all six peptides in different media, including aqueous solutions and membrane-like environments (Fig. 2). In sodium phosphate buffer, GW10, indolicidin (IN13) and GW13 displayed spectra typical of an unordered conformation (Fig. 2a, b, f). However, the peptides GW16, GW19, and GW22 showed a range of secondary structures, and the spectra suggested a population with helical conformation. Furthermore, in 30 mM SDS, used usually to mimic the negatively charged prokaryotic membrane, the CD spectra of GW10 and GW13 were less obvious, while greater RWL-content peptides showed improved CD spectra, displaying more α-helical-rich structure characterized by the positive bands near 195 nm and the dichroic minimal values at 205–208 and 222–223 nm (Fig. 2c–e).

Antimicrobial activity

The antimicrobial activities of the peptides were tested in terms of their bacteriostatic inhibitory concentrations, indicated by the MIC, as summarized in Table 2. The peptides' ability to inhibit growth of these microbial cells displayed regular changes with RWL multiplicity. The relationship between the lengths of H-$(RWL)_n$ AMPs and antibacterial activity can be fit to a linear regression equation described by a quadratic function (Fig. 3a). The

Table 2 Minimum inhibitory concentrations (MIC), minimum hemolytic concentrations (MHC), and therapeutic indices (TI) of the peptides against gram-negative and gram-positive bacterial strains

Peptide	MIC[a] (μM)								GM[b] (μM)	MHC[c] (μM)	TI[d]
	Gram negative				Gram positive						
	E. coli	*S. Pullorum*	*S.* Typhimurium	*B. yocyaneum*	*S. aureus*	*S. epidermidis*	*S. faecalis*	*B. subtilis*			
GW10	>128	>128	>128	>128	>128	>128	>128	>128	256	>128	1.0
GW13	4	4	4	8	4	8	16	2	5.2	128	24.6
GW16	8	1	4	32	8	8	4	2	5.2	2	0.4
GW19	16	>128	8	>128	4	2	>128	0.5	17.4	0.5	<0.1
GW22	>128	>128	8	>128	8	>128	>128	2	47.6	0.25	<0.1
IN13	8	16	8	>128	4	8	128	1	13.5	32	2.4

[a] MICs were determined as the lowest concentration of peptide that prevented visible turbidity

[b] The geometric mean (GM) of the peptide MICs against all four bacterial strains was calculated. When no detectable antimicrobial activity was observed at 128 μM, a value of 256 μM was used to calculate the therapeutic index

[c] MHC is the minimum hemolytic concentration that caused 10 % hemolysis of human red blood cells (hRBC). When no detectable hemolytic activity was observed at 128 μM, a value of 256 μM was used to calculate the therapeutic index

[d] Therapeutic index (TI) is the ratio of the MHC to the geometric mean of MIC (GM). Larger values indicate greater cell selectivity

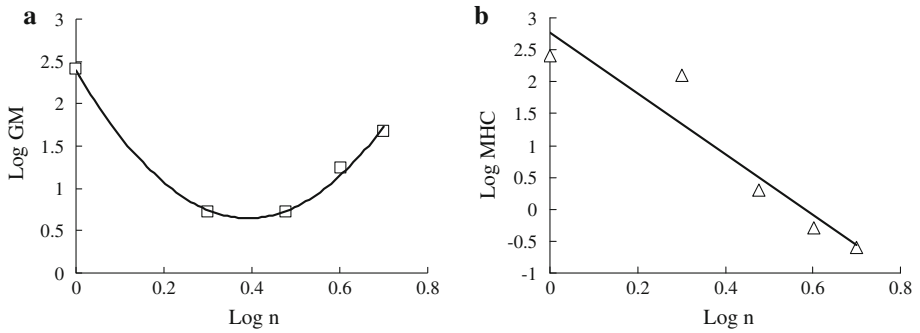

Fig. 3 Correlation between biological activities and the multiplicity of RWL. **a** The data can be fit to a power law between the antimicrobial activity (GM) and the number of RWL repeats (1, 2, 3, 4, or 5) in the peptides as log GM = a(log n)^2 − b(log n) + c, with a, b, and c equal to 11.42, 8.94, and 2.40 (R^2 = 0.99), respectively. **b** Log GM is replaced by log MHC to obtain a linear correlation, and the data can be fit to a power law as log MHC = a(log n) + b, with a and b equal to −4.76 and 2.576 (R^2 = 0.90), respectively

potency of antimicrobial activity was ranked according to the geometric mean of the MICs as follows: GW13 = GW16 > GW19 > GW22 > GW10. GW13 and GW16, with an overall MIC of 5.2 μM across the bacterial species, had approximately twofold greater antimicrobial activity than IN13. The shortest peptide, GW10, had no antimicrobial activity in the range of concentrations tested.

Hemolytic activity

Generally, the application of biomaterials as anti-infective agents needs to be evaluated for undesirable cytotoxicity. The cytotoxicity of synthetic AMPs is often analyzed in terms of their ability to lyse mammalian red blood cells, referred to as hemolysis. The ability of the peptides tested in this study to induce hemolysis of human erythrocytes is summarized in Table 2. The relationship between the lengths of H-(RWL)$_n$ AMPs and hemolytic activity can be fit to a linear regression equation (Fig. 3b). The one- and two-RWL-tagged peptides GW10 and GW13 had no hemolytic activity at concentrations as high as 128 μM. RWL-tagged peptides of higher multiplicity can cause the lysis of human erythrocytes; GW16, GW19 and GW22 had 10 % hemolytic activity at 2, 0.5, and 0.25 μM, respectively.

The therapeutic index (TI) is calculated by the ratio of MHC (the peptide concentration that causes 10 % hemolysis) to MIC and was used to evaluate cell selectivity. As shown in Table 2, GW13 exhibited a great TI of 24.6, offering optimal selectivity. GW16 had a lower TI of 0.4; GW19 and GW22 had the lowest TIs, valued at <0.1.

Mechanism of antibacterial activity

The fluorescence emission characteristics of the Trp residues in these pore forming peptides are sensitive to their environment and were used to monitor the binding of

Table 3 Fluorescence spectroscopy parameters measured for the peptides in the presence and absence of PE/PG and PC/cholesterol vesicles

Peptide	Fluorescence emission maxima (nm)[a]			K_{SV}[b] (M^{-1})		
	Buffer	PE/PG	PC/cholesterol	Buffer	PE/PG	PC/cholesterol
GW10	350	345 (5)	349 (1)	7.82	1.21	2.00
GW13	350	335 (15)	345 (5)	12.05	1.04	2.83
GW16	351	337 (14)	341 (10)	12.29	1.42	2.14
GW19	350	339 (11)	341 (9)	15.52	1.33	2.03
GW22	350	347 (3)	343 (7)	13.99	1.44	1.81
IN13	350	335 (15)	342 (8)	10.09	1.76	2.27

[a] Blue shift of emission maximum as compared to Tris buffer

[b] Stern–Volmer constant K_{SV} was calculated by the Stern–Volmer equation: $F_0/F = 1 + K_{SV}(Q)$, where Q is the concentration of the quencher (acrylamide). Concentrations of the quencher were increased from 0.01 to 0.40 M. A smaller K_{SV} value reflects a more protected Trp residue

peptides to lipid vesicles. The liposomal PE/PG and PC/cholesterol vesicles generally mimic bacterial and eukaryotic membranes, respectively. The varying degrees of fluorescence emission spectra for the tryptophan of all H-$(RWL)_n$ peptides in the presence of phospholipid vesicles are shown in Table 3. All peptides caused maximal fluorescence emission at approximately 350 nm in aqueous solutions. The blue shifts in PE/PG vesicles first increased and then decreased with increasing multiplicity of the RWL trimer, which correlated with the antimicrobial activity of these peptides. The two-RWL-tagged peptide GW13 induced larger blue shifts in PE/PG than in PC/cholesterol vesicles, which was consistent with its biological activity. Little or no blue shift was observed in PE/PG or PC/cholesterol vesicles for GW10, correlating with its lack of antimicrobial and hemolysis activity of the peptide.

The location of the peptides with respect to the bilayer plane was further investigated using fluorescence quenching techniques to create Stern–Volmer plots of the decrease in fluorescence as a function of an added soluble quencher. GW13 does not only have the highest K_{SV} in negatively charged vesicles but also the lowest value in uncharged vesicles as compared to the other peptides, which was in agreement with its greatest cell specificity among the detected peptides.

Based on the MIC and MHC values and tryptophan fluorescence emission of the peptides, the potential use of GW13 is more promising than the other peptides tested. Hence, the mechanisms of action were further studied by observing the integrity of the bacterial cell membrane after treatment with this peptide. Propidium iodide staining of nucleic acids in cells is indicative of compromised cell membrane permeability and cell death. Therefore, flow cytometric analysis was used to determine membrane integrity (Fig. 4). This analysis demonstrated that the control (no peptide) resulted in only 3.9 % PI-positive cells. The percentage of PI-positive cells with membranes damaged by GW13 was 71.5 % (1/2 × MIC), 80.0 % (1 × MIC), and 89.0 % (2 × MIC). IN13 treatment resulted in positive nucleic acid staining of 26.9 % (1/2 × MIC), 66.7 % (1 × MIC), and 83.9 % (2 × MIC). Both peptides damaged the cell membrane in a dose-dependent manner, but GW13 caused a greater accumulation of PI than IN13.

To more precisely examine the interaction of the peptide with the bacterial cell membrane in vitro, FITC-labeled GW13 was incubated with *E. coli*, and peptide distribution in the bacteria was investigated by confocal laser-scanning microscopy (Fig. 5). At 1 × MIC, not all cells displayed green fluorescence, while at a concentration greater than 2 × MIC, FITC-labeled GW13 can completely penetrate the cell membrane and accumulate inside *E. coli*, suggesting that a direct interaction and membrane penetration are needed in the bactericidal mechanism.

The surface morphology of the bacteria was further evaluated by FE-SEM microscopy (Fig. 6). These images show that the integrity of *E. coli* and *S. aureus* cells' membranes were grossly affected upon the treatment with GW13 or IN13 for 60 min at 1 × MIC. The membrane surface of peptide-treated *E. coli* cells became shrinkage, changing the overall morphology of the bacterial cells (Fig. 6a). For comparison, the effect of these peptides on *S. aureus* is shown in Fig. 6e, f. The cell surface became obviously roughened and decorated with discrete blebs when treated with the peptides. Moreover, the more severe loss of membrane integrity was found in the GW13-treated cells than IN13-treated cells.

Antitumor activity

Many natural antibacterial peptides have antitumor activity, so we also tested the antitumor activity of our peptides by observing the proliferation of human embryonic lung fibroblast MRC-5 and human hepatocellular carcinoma

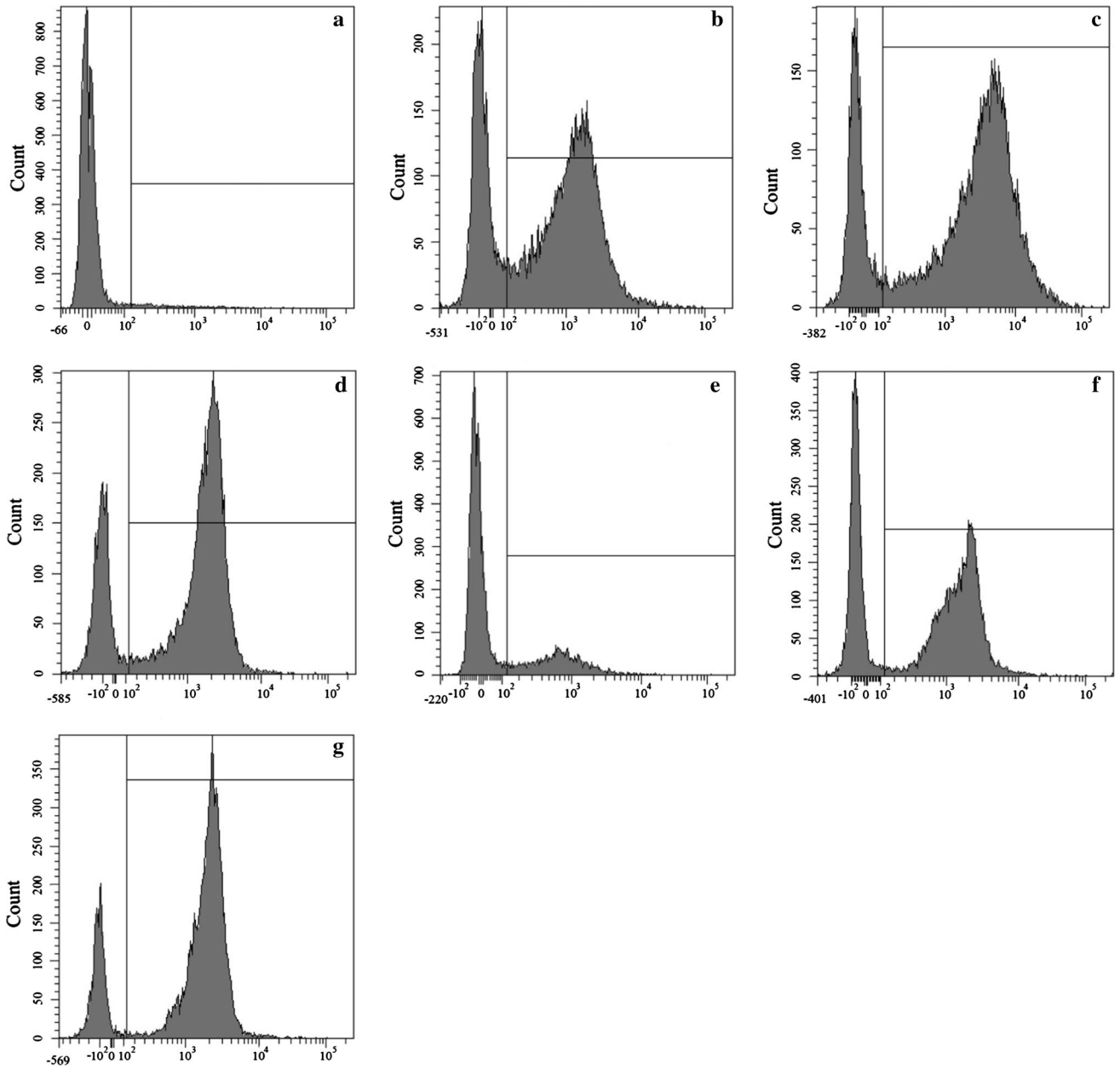

Fig. 4 Flow cytometric analysis. Exponential phase *E. coli* cells were treated with GW13, and cellular fluorescence was analyzed by flow cytometry. The increments of the log fluorescence signal represent PI uptake resulting from peptide treatment. **a** No peptide, negative control; **b** GW13 (1/2 × MIC, 2 μM); **c** GW13 (1 × MIC, 4 μM); **d** GW13 (2 × MIC, 8 μM); **e** IN13 (1/2 × MIC, 4 μM); **f** IN13 (1 × MIC, 8 μM); **g** IN13 (2 × MIC, 16 μM)

HepG2 cells, using the well-established MTT assay. Figure 7 shows the survival rate in the peptide concentration range of 1–128 μM. The dose–response studies revealed that longer peptides (GW16, GW19 and GW22) displayed significantly greater cytocidal activities toward MRC-5 and HepG2 cells as compared to the shorter peptides GW10 and GW13. Moreover, the concentration of peptides that completely inhibited the growth of HepG2 cells was lower than that of MRC-5 cells. At the highest concentration of 128 μM, the survival rates of GW10- and GW13-treated MRC-5 cells were 93 and 81 %, while rates for HepG2 cells were 94 and 3 % respectively. GW16, GW19 and GW22 had maximal cytotoxicity leading to near-zero cell viability. Compared to the other peptides, GW13 has the greatest selectivity between normal cells and cancer cells. Thus, based on its lower cytotoxicity toward the human fibroblastic cell line, we selected GW13 for further investigation of the mechanism of action.

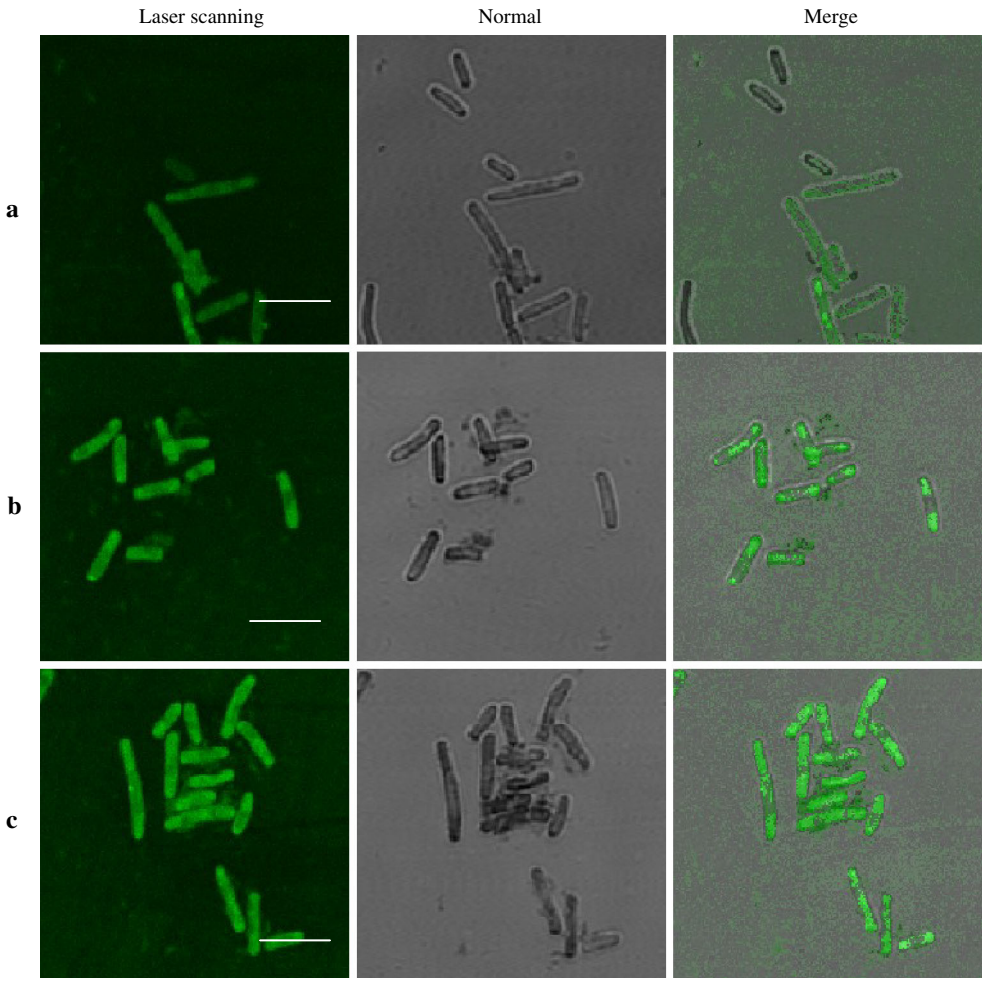

Fig. 5 Confocal laser-scanning microscopy of *E. coli* treated with FITC-labeled peptides. The cells were treated with FITC-labeled GW13. **a** 1 × MIC, 4 μM; **b** 2 × MIC, 8 μM; **c** 5 × MIC, 20 μM; *scale bar* 2 μm

Antitumor mechanism

To better understand the mechanism of these peptides against HepG2 cells, we measured the apoptosis of HepG2 cells by an Annexin-V-FITC/PI assay. Phosphatidylserine (PS), in the early stage of apoptosis, shifts from the inside of the plasma membrane to the outer layer. Annexin-V, a calcium-dependent phospholipid-binding protein, binds to PS with high affinity, and this binding is a marker of cell apoptosis. The results of cell apoptosis measurement are shown in Fig. 8. The Q_1 gate represents cell necrosis, Q_2 represents the late stage of apoptosis, Q_3 represents normal cells, and Q_4 represents the early stage of apoptosis. Collectively, these results showed that early-stage apoptosis was induced concentration-dependently up to 32 μM, while higher concentrations greatly promoted late-stage apoptosis.

The apoptotic vesicular fragments and the holes in the HepG2 cell membranes after treatment with GW13 were further examined by SEM, with representative images shown in Fig. 9. The untreated HepG2 cells had long and thin microvilli on the cell surfaces. In contrast, the GW13-treated cells showed pronounced shrinkage and the loss of microvilli when the concentration exceeded 32 μM. The cell surface became covered with blebs at 64 μM, which may be attributed to leakage of cytoplasmic contents (Fig. 9c). The morphology changed drastically for HepG2 cells treated with 128 μM of GW13, causing many visible holes (Fig. 9d). Thus, both fluorescence and SEM studies confirmed that GW13 could cause cell death through apoptosis and membrane disruption.

Subsequently, morphological characterization of HepG2 cell apoptosis was further analyzed by Hoechst 33258/PI double staining, with the results shown in Fig. 10. Hoechst 33258, a fluorescence dye used to assess membrane permeability, was used to examine apoptotic cells by changes in nuclear morphology such as chromatin condensation and fragmentation, and PI was used to examine the late stages

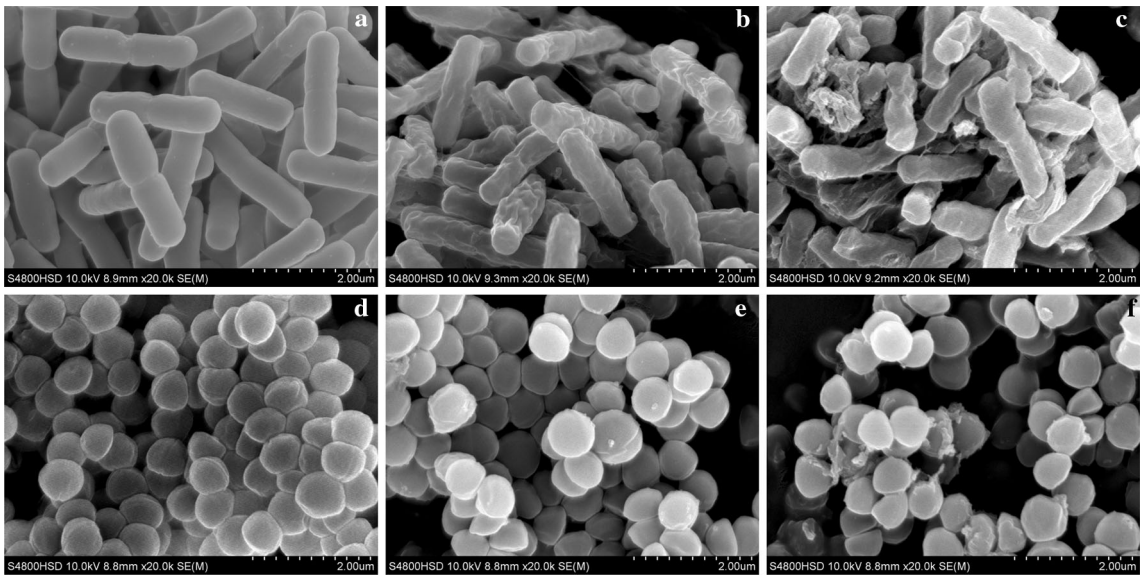

Fig. 6 SEM micrographs of *E. coli* 25922: **a** control; **b** IN13 treated; **c** GW13 treated. SEM micrographs of *S. aureus* 29213: **d** control; **e** IN13 treated; **f** GW13 treated. Bacteria were treated with peptides at 1 × MIC for 1 h. The control was performed without peptides

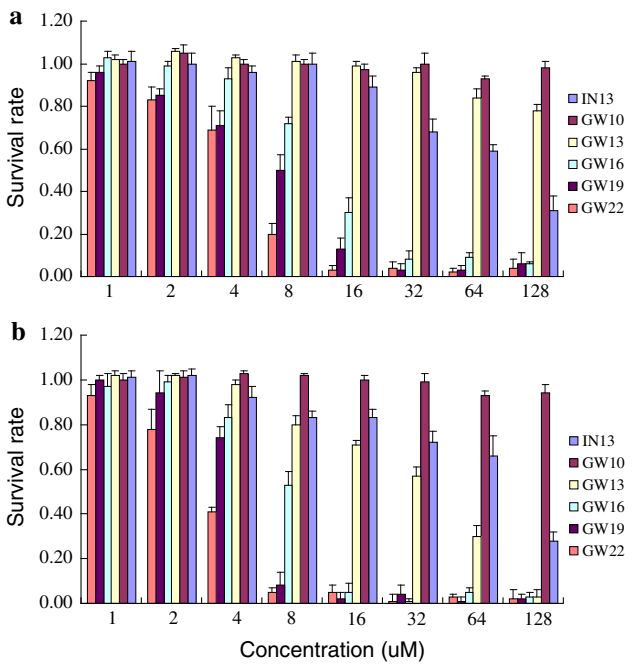

Fig. 7 Viability of MRC-5 (**a**) and HepG2 (**b**) cells in the absence or presence of the peptides ($P < 0.05$)

of apoptosis and necrosis in cells. Nuclei were stained blue by Hoechst 33258 and red by PI. Figure 10 shows representative Hoechst 33258/PI fluorescence photomicrographs of cultured HepG2 cells treated with or without GW13. In the control and the 8 μM GW13-treated groups, the majority of nuclei were stained only blue with a normal appearance (Fig. 10a, b). In contrast, most nuclei of the cells treated with 64 μM GW13 were smaller with visibly condensed chromatin (Fig. 10e). When 128 μM GW13 was added (Fig. 10f), the cells' nuclei contained both dyes, indicating that the cells were in late-stage apoptosis or necrosis.

The loss of mitochondrial membrane potential is a characteristic of cell apoptosis. JC-1 accumulates and aggregates in the mitochondria (red) in non-apoptotic cells and exists as a monomer in the cytosol (green) in apoptotic and necrotic cells. Figure 11 shows representative JC-1 staining of apoptotic and non-apoptotic HepG2 cells. In the negative control (0 μM) groups (Fig. 11a), most HepG2 cells showed red fluorescence, indicating that they were alive. In 16 and 32 μM GW13 groups (Fig. 11b, c), yellow-green HepG2 cells gradually increased, indicating that some cells were apoptotic or necrotic. However, we observed a significant change in JC-1 staining in the HepG2 cells after 64 and 128 μM treatments similar to the positive control CCCP, suggesting GW13-induced HepG2 cell necrosis or apoptosis.

Discussion

As the incidence of antibiotic resistance in pathogenic bacteria rises worldwide, there exists an urgent need for new antimicrobial agents with activity against multidrug-resistant pathogens (Rice 2003). AMPs represent a novel class of antibiotic agents that may be useful in the treatment of a range of infectious diseases (Hancock and Lehrer 1998). The unique mechanism by which AMPs kill bacteria is through the targeting and disruption of the plasma

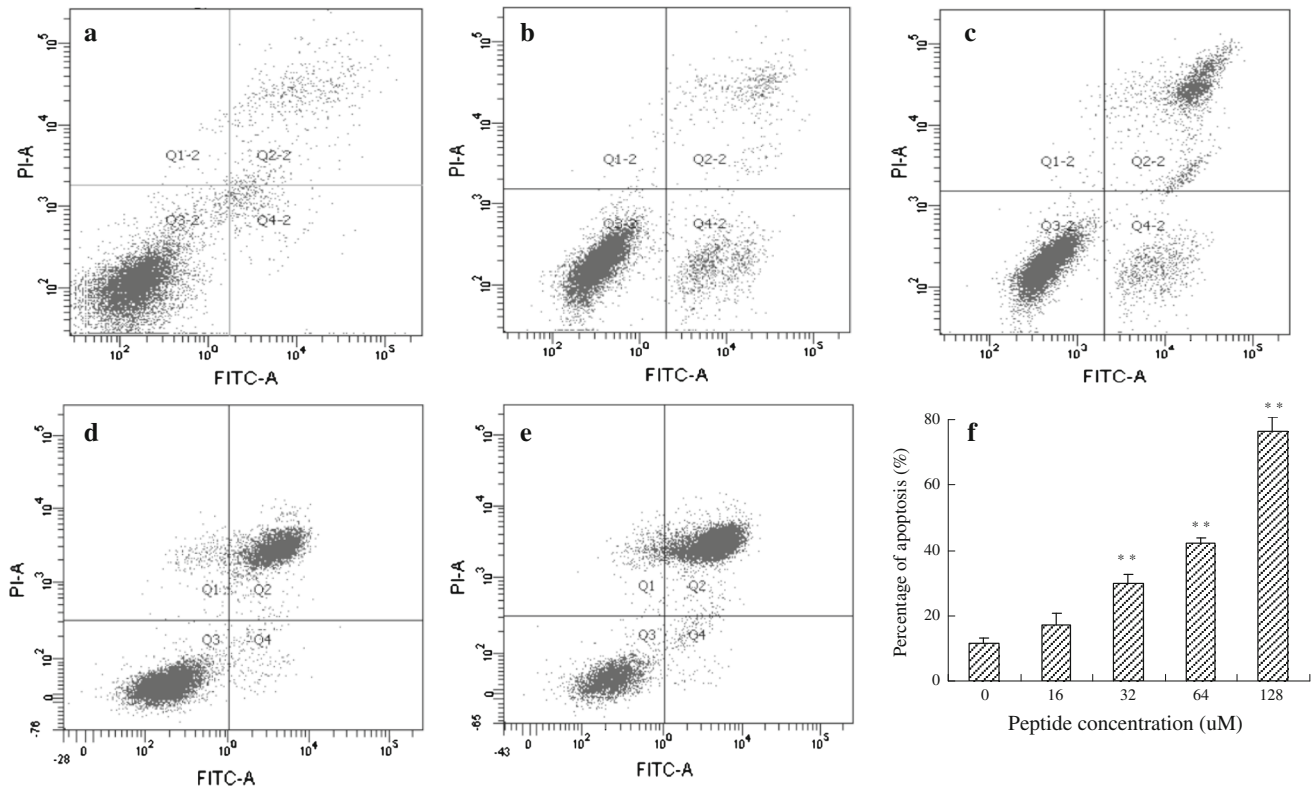

Fig. 8 Effects of GW13 on HepG2 cells determined by Annexin-V-FITC and propidium iodide double staining. *Representative dot plots* of Annexin-V/PI staining are shown. HepG2 cells were treated for 24 h with or without the addition of GW13. **a** 0 μM (the control); **b** 16 μM; **c** 32 μM; **d** 64 μM; **e** 128 μM; **f** quantitative analysis of Annexin-V/PI staining normalized to the control. The results are expressed as the mean ± SD from three independent experiments. (**$P < 0.01$ compared to the control group)

membrane, which may help to overcome antibiotic resistance of bacteria. However, natural antibacterial peptides extracted from organisms often suffer from problems such as high production cost and hemolytic activity, along with possible immunological responses (Hancock and Sahl 2006; Wang et al. 2010; Chen et al. 2010). To avoid these inherent limitations and develop novel AMPs, new techniques need to be used, including optimizing the selectivity of peptides by controlling critical biophysical parameters such as positive charge, hydrophobicity and amphiphilicity (Sitaram and Nagaraj 1999; Chen et al. 2007). A net positive charge favors peptide binding to the negatively charged membranes of bacterial and cancer cells, and hydrophobicity promotes insertion into membranes. Slight modifications in the balance of net positive charge and hydrophobicity can give rise to marked changes in antimicrobial selectivity/activity (Zelezetsky et al. 2005). Many researchers are dedicated to the study of relationships between these parameters and the biological activities of antibacterial peptides to determine optimal rational design of peptides by primary structure modification (Selsted et al. 1992), introduction of amino acid point mutations (Subbalakshmi et al. 2000), and hybridization (Liu et al. 2013).

Recently, the repeated permutation of specific amino acids within AMPs has been an effective strategy for the design of novel AMPs (Liu et al. 2007; Niidome et al. 2005; Deslouches et al. 2005). Most studies have focused on the use of several simple amino acid sequences in repetition to design amphipathic peptides. In the current study, the amino acid sequence from the natural antibacterial peptide AvBD-4 was introduced into a series of peptides H-$(RWL)_n$. The RWL is the trimeric amino acid sequence at the C-terminal of AvBD-4, and repeated attachment of the RWL acyl chain can alter antimicrobial activity and selectivity. The results displayed that the relationship between the lengths of H-$(RWL)_n$ AMPs and antibacterial activity was described by a quadratic function, while the hemolytic activity can be fit to a linear regression equation (Fig. 3). Our previous results showed that the antimicrobial activity of β-hairpin-like AMPs initially increased and then decreased with chain length, similar to what is shown here (Dong et al. 2012c). Our results indicated that adding a trimeric RWL sequence with one charged residue R and two bulky or hydrophobic residues W or L can improve the antibacterial activity; greater extension does not raise these indices. Strom et al. have proven that tryptophan provides better bulk and

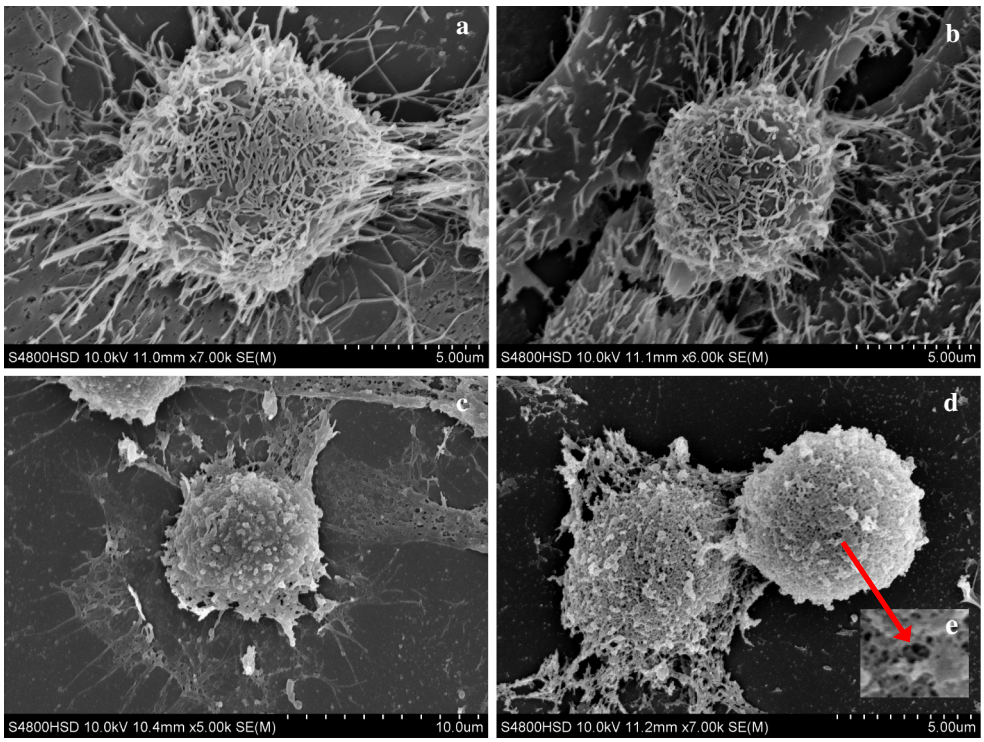

Fig. 9 Examining the effect of GW13 on the cell membranes of HepG2 cells using scanning electron microscopy for 24 h. SEM micrographs of **a** control HepG2 cells; **b** 32 μM; **c** 64 μM; **d** 128 μM; **e** micrograph magnification was ×10

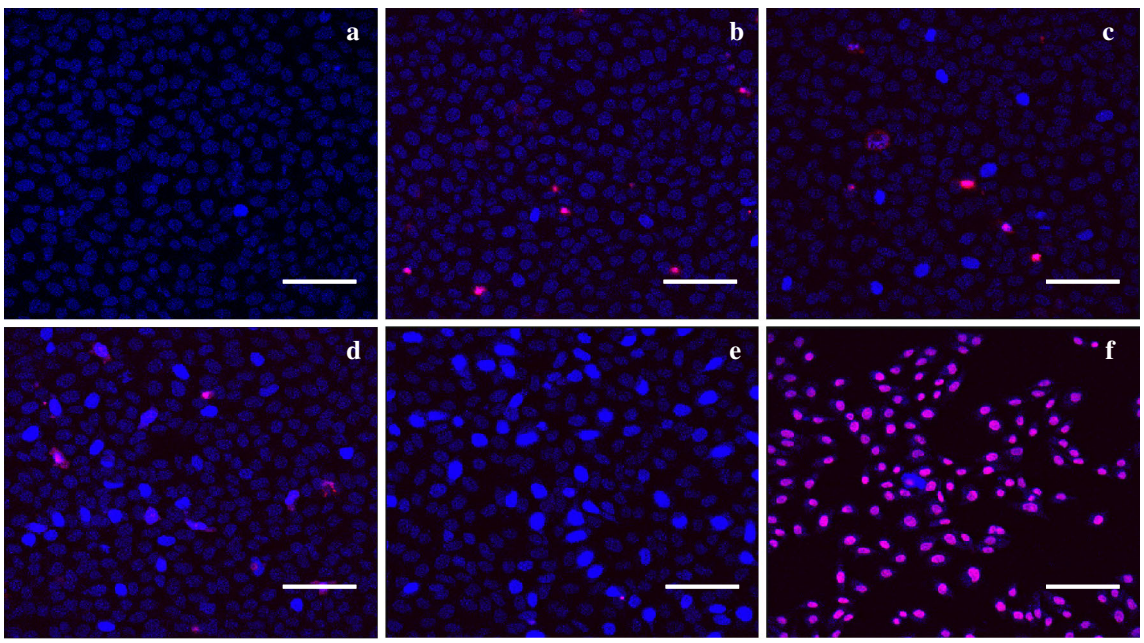

Fig. 10 HepG2 cells were treated for 24 h with or without the addition of GW13. Fluorescence photomicrograph of HepG2 cells stained with Hoechst 33258/PI. HepG2 cells were exposed to no peptide as control (**a**), 8 μM (**b**), 16 μM (**c**), 32 μM (**d**), 64 μM (**e**) and 128 μM (**f**) GW13 for 24 h; *scale bar* 100 μm

lipophilicity than tyrosine, and a minimum of two tryptophan and charged residues are required to be present to give activity against *staphylococci*, with *Escherichia coli* requiring an additional bulky amino acid (Strom et al. 2003). The lack of antimicrobial activity with GW19 or GW22 may be related to the fact that the RWL-peptide

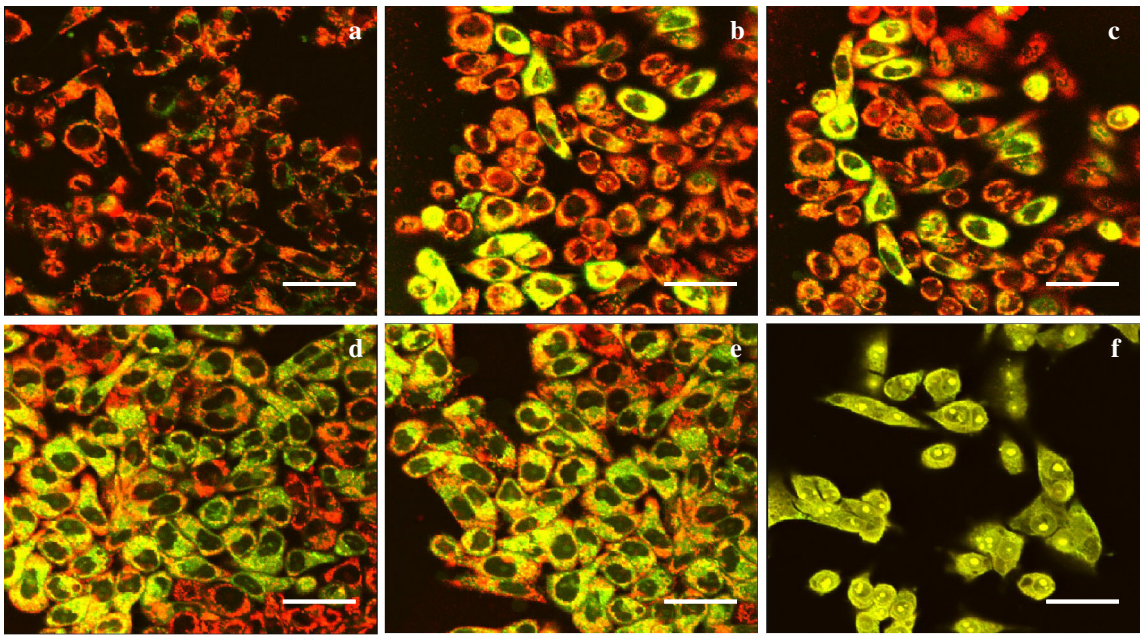

Fig. 11 Representative laser-scanning confocal microscopy photographs of JC-1 staining after treatment with different concentrations of GW13 for 24 h. **a** control; **b** 16 μM; **c** 32 μM; **d** 64 μM; **e** 128 μM; **f** CCCP; *scale bar* 20 μm

appears to oligomerize in solution, and the oligomers may be too large to pass through the bacterial membrane of specific bacteria (*S. Pullorum, B. yocyaneum, and S. faecalis*). Generally, a great propensity for aggregation is found in aqueous buffers due to the increased hydrophobicity (Yin et al. 2012). Interestingly, in the current study, GW19 and GW22 may show aggregation involving no significant increase of the peptides' hydrophobic value. Our Trp blue-shift assays and quenching experiments showed that their aggregation state may lead longer chain peptides to bind more weakly to membranes than GW13 with its optimal selectivity does, which would also reduce their ability to penetrate the membrane. Amphipathicity is often cited as an important factor that contributes to the effectiveness of AMPs (Haney et al. 2009). The 13-mer AMP GW13, with low cytotoxicity to mammalian cells (Fig. 7), has the highest amphiphilic parameter (the mean hydrophobicity moment is 1.25) among all five RWL-tagged peptides, and exerted optimal antimicrobial activity. As a control peptide, indolicidin (IN13), isolated from the cytoplasmic granules of bovine neutrophils (Selsted et al. 1992), has the same amino acid number (13) as GW13. IN13 displays activity against gram-positive and gram-negative bacteria, but the relatively high toxicity toward mammalian cells prevents its use as an antibiotic. It is notable that GW13 had significantly lower cytotoxicity to mammalian cells than IN13, suggesting that GW13 has the potential to become an antibiotic replacement.

Previous studies reported that natural amphiphilic AMPs display random structure in aqueous solutions and assemble into a pattern of α-helical or β-sheet structure in the presence of a membrane-like environment. To investigate the conformational structures of the RWL-containing peptides in both water- and membrane-like environments, the peptides were analyzed by CD spectroscopy at room temperature, using sodium phosphate buffer and 30 mM SDS micelles as the solvent environment (Fig. 2). Our results demonstrated that the greater multiplicity RWL-peptide structures displayed more helical conformation in both solutions. Especially, in SDS, the CD spectra of the peptides (more than one trimeric RWL) displayed obvious α-helical-rich structure. This finding suggests that greater RWL-content-associated α-helix structure acquisition may account for gradually increasing the cytotoxicity.

Most AMPs with cationic and amphipathic properties can disrupt membranes or form pore/ion channels in the cytoplasmic membranes of pathogenic bacteria (Sato and Feix 2006). In the present study, the membrane integrity data, based on FACScan analysis (Fig. 4), confirmed that GW13 exhibited greater membrane penetration potential than IN13, which was in agreement with antimicrobial activities of these peptides. Our SEM studies further demonstrated that GW13 caused pronounced vesiculation of the outer membrane (Fig. 6), indicating that GW13 caused large lesions in the cell envelope and membrane blebbing or shriveling due to leakage of cytosolic fluid and suggesting that GW13 kills bacteria via membrane disruption. IN13 showed similar membrane disturbance, but to a lesser extent, consistent with its reduced microbicidal

capacity. Previous research has shown that IN13 kills bacteria through the carrier-type mechanism of efflux rather than formation of aqueous pores (Subbalakshmi and Sitaram 1998). Unlike IN13, GW13 exerts its bactericidal activity by destroying the membrane by carpeting or pore formation, leading to leakage of the cytosol and eventually lysing the whole cell. To further estimate the peptide localization after entering the bacterial cell membrane, confocal laser-scanning microscopy of FITC-labeled GW13-treated *E. coli* was performed, and the results showed that GW13 penetrated the cell membrane and accumulated in the cytoplasm (Fig. 5).

In this study, the results demonstrated that GW13 had highly selective toxicity, which may involve selective membrane action between the tumor cell membrane and the normal cell membrane. The mechanism of cell death of HepG2 cells after GW13 exposure in vitro was evaluated by the data obtained from cell viability (Fig. 7), exposure of PS on the cell membrane by Annexin-V-FITC/PI double staining (Fig. 8), chromatin condensation by Hoechst 33258/PI staining, and mitochondrial membrane potential (Fig. 10). SEM was used to visualize the morphological changes of HepG2 cells treated with GW13 (Fig. 9). The results displayed that the membranes of tumor cells treated with GW13 were disrupted, which was similar to previous studies that showed membrane-active antibacterial peptides can bind rapidly to and disrupt the plasma membrane of tumor cells, leading to cell death (Riedl et al. 2011). The negatively charged components of the cancer cell membranes and the greater membrane fluidity and cell surface area were thought to play an important role in attracting the cationic AMPs to the plasma membrane of the tumor cells (Hoskin and Ramamoorthy 2008). In addition, *O*-glycosylated mucin, a type of glycoprotein, exists in cancer cell membranes and can increase negative charges on cancer cell surfaces (Yoon et al. 1996). However, normal mammalian cell membranes are primarily composed of neutral zwitterionic phospholipids and sterols (Cruciani et al. 1991). Therefore, AMPs typically contain positive charges; GW13 has eight net charges, so anionic cancer cell membranes are more susceptible to the lytic action of the AMPs. Also, AMPs containing hydrophobic residues are able to penetrate the cancer cell membrane and damage it. It is very likely that the basic mechanism by which AMPs act on microbes is comparable to the mechanism in tumor cells.

To investigate whether the cytotoxic effects of GW13 were related to changes in the mitochondrial transmembrane potential, the intensity and shift of fluorescence emission of the JC-1 dye were monitored by flow cytometry. CCCP, an uncoupler of oxidative phosphorylation (Banki et al. 1999) known to trigger loss of mitochondrial membrane potential, was used as a positive control. In this study, there was a significant fluorescence change between the GW13-treated group and the untreated group (Fig. 11). This result demonstrated that the disruption of mitochondrial membrane potential by GW13 induced apoptosis in HepG2 cells.

Conclusion

In this study, we have highlighted that tethering three-unit amino acid repeats (RWL) onto a natural amino acid sequence can produce potential AMPs that can kill both bacterial and tumor cells, while remaining benign to host mammalian cells, as evident from low cytotoxicity to RBCs and MRC-5 cells. This high selectivity was attributed to favorable cationic charge and amphiphilicity of the peptides, providing affinity to the negatively charged outer cell membranes (common to both bacteria and tumor cells) where hydrophobic amino acids could ultimately damage the cell membrane. Among the series of peptides studied, the peptide with two-RWL units, GW13, provides the highest selectivity towards a wide range of microbes. The mechanism of action against bacteria was determined through combined SEM and fluorescence assays, revealing that the peptide kills bacterial cells by damaging the cell membrane. The antitumor mechanism of this peptide in HepG2 cells involved not only pore formation and selective membrane disruption, but also apoptosis confirmed by a series of fluorescence assays. Although the in vitro results with RWL-containing peptides show potential antibacterial and antitumor selectivity, in vivo models will also need to be used, in which diverse technological applications such as biomedical coatings, cosmetics, and food storage can be explored.

Acknowledgments This work was supported financially by the National Basic Research Program (2012CB124703), the National Natural Science Foundation of China (31272453), the China Agriculture Research System (CARS-36), the Postgraduate Innovative Research Projects of Heilongjiang Province (YJSCX2012-004HLJ), and the Open Projects of Key Laboratory of Feed Science, College of Heilongjiang Province (yy-2012-03).

Conflict of interest We have no proprietary, financial, professional or other personal interest of any nature or kind in any product, service and/or company that could be construed as influencing the position presented in, or the review of, the manuscript entitled: “Cell specificity and molecular mechanism of antibacterial and antitumor activities of carboxyl-terminal RWL-tagged antimicrobial peptides”.

References

Banki K, Hutter E, Gonchoroff NJ, Perl A (1999) Elevation of mitochondrial transmembrane potential and reactive oxygen intermediate levels are early events and occur independently from activation of caspases in Fas signaling. J Immunol 162(3):1466–1479

Bell A (2011) Antimalarial peptides: the long and the short of it. Curr Pharm Des 17(25):2719–2731

Bell G, Gouyon PH (2003) Arming the enemy: the evolution of resistance to self-proteins. Microbiology 149(Pt 6):1367–1375

Beven L, Castano S, Dufourcq J, Wieslander A, Wroblewski H (2003) The antibiotic activity of cationic linear amphipathic peptides: lessons from the action of leucine/lysine copolymers on bacteria of the class Mollicutes. Eur J Biochem 270(10):2207–2217

Burkert U, Allinger NL (1982) Molecular mechanics, vol 177. American Chemical Society, Washington DC

Chen Y, Guarnieri MT, Vasil AI, Vasil ML, Mant CT, Hodges RS (2007) Role of peptide hydrophobicity in the mechanism of action of alpha-helical antimicrobial peptides. Antimicrob Agents Chemother 51(4):1398–1406

Chen C, Pan F, Zhang S, Hu J, Cao M, Wang J, Xu H, Zhao X, Lu JR (2010) Antibacterial activities of short designer peptides: a link between propensity for nanostructuring and capacity for membrane destabilization. Biomacromolecules 11(2):402–411

Chen C, Hu J, Zhang S, Zhou P, Zhao X, Xu H, Zhao X, Yaseen M, Lu JR (2012) Molecular mechanisms of antibacterial and antitumor actions of designed surfactant-like peptides. Biomaterials 33(2):592–603

Cruciani RA, Barker JL, Zasloff M, Chen H-C, Colamonici O (1991) Antibiotic magainins exert cytolytic activity against transformed cell lines through channel formation. Proc Natl Acad Sci USA 88(9):3792–3796

Dathe M, Nikolenko H, Klose J, Bienert M (2004) Cyclization increases the antimicrobial activity and selectivity of arginine- and tryptophan-containing hexapeptides. Biochemistry 43(28):9140–9150

Deslouches B, Phadke SM, Lazarevic V, Cascio M, Islam K, Montelaro RC, Mietzner TA (2005) De novo generation of cationic antimicrobial peptides: influence of length and tryptophan substitution on antimicrobial activity. Antimicrob Agents Chemother 49(1):316–322

Dong N, Ma Q–Q, Shan A-S, Lv Y-F, Hu W, Gu Y, Li Y-Z (2012a) Novel design of short antimicrobial peptides derived from the bactericidal domain of avian-defensin-4. Protein Pept Lett 19(11):1212–1219

Dong N, Ma Q–Q, Shan A-S, Wang L, Sun W-Y, Li Y-Z (2012b) Influence of truncation of avian-defensin-4 on biological activity and peptide-membrane interaction. Protein Pept Lett 19(4):430–438

Dong N, Ma Q, Shan A, Lv Y, Hu W, Gu Y, Li Y (2012c) Strand length-dependent antimicrobial activity and membrane-active mechanism of arginine- and valine-rich beta-hairpin-like antimicrobial peptides. Antimicrob Agents Chemother 56(6):2994–3003

Guillen Schlippe YV, Hartman MC, Josephson K, Szostak JW (2012) In vitro selection of highly modified cyclic peptides that act as tight binding inhibitors. J Am Chem Soc 134(25):10469–10477

Hancock RE, Lehrer R (1998) Cationic peptides: a new source of antibiotics. Trends Biotechnol 16(2):82–88

Hancock RE, Sahl HG (2006) Antimicrobial and host-defense peptides as new anti-infective therapeutic strategies. Nat Biotechnol 24(12):1551–1557

Haney EF, Hunter HN, Matsuzaki K, Vogel HJ (2009) Solution NMR studies of amphibian antimicrobial peptides: linking structure to function? Biochim Biophys Acta 1788(8):1639–1655

Hoskin DW, Ramamoorthy A (2008) Studies on anticancer activities of antimicrobial peptides. Biochim Biophys Acta 1778(2):357–375

Hu H, Xue J, Swarts BM, Wang Q, Wu Q, Guo Z (2009) Synthesis and antibacterial activities of N-glycosylated derivatives of tyrocidine A, a macrocyclic peptide antibiotic. J Med Chem 52(7):2052–2059

Hu J, Chen C, Zhang S, Zhao X, Xu H, Zhao X, Lu JR (2011) Designed antimicrobial and antitumor peptides with high selectivity. Biomacromolecules 12(11):3839–3843

Ladokhin AS, White SH (1999) Folding of amphipathic alpha-helices on membranes: energetics of helix formation by melittin. J Mol Biol 285(4):1363–1369

Lee KH, Lee DG, Park Y, Kang DI, Shin SY, Hahm KS, Kim Y (2006) Interactions between the plasma membrane and the antimicrobial peptide HP (2-20) and its analogues derived from *Helicobacter pylori*. Biochem J 394(Pt 1):105–114. doi:10.1042/Bj20051574

Liu Z, Brady A, Young A, Rasimick B, Chen K, Zhou C, Kallenbach NR (2007) Length effects in antimicrobial peptides of the $(RW)_n$ series. Antimicrob Agents Chemother 51(2):597–603

Liu Y, Xia X, Xu L, Wang Y (2013) Design of hybrid beta-hairpin peptides with enhanced cell specificity and potent anti-inflammatory activity. Biomaterials 34(1):237–250

Niidome T, Matsuyama N, Kunihara M, Hatakeyama T, Aoyagi H (2005) Effect of chain length of cationic model peptides on antibacterial activity. Bull Chem Soc Jpn 78(3):473–476

Rice LB (2003) Do we really need new anti-infective drugs? Curr Opin Pharmacol 3(5):459–463

Riedl S, Zweytick D, Lohner K (2011) Membrane-active host defense peptides–challenges and perspectives for the development of novel anticancer drugs. Chem Phys Lipids 164(8):766–781

Rubinchik E, Dugourd D, Algara T, Pasetka C, Friedland HD (2009) Antimicrobial and antifungal activities of a novel cationic antimicrobial peptide, omiganan, in experimental skin colonisation models. Int J Antimicrob Agents 34(5):457–461

Sato H, Feix JB (2006) Peptide-membrane interactions and mechanisms of membrane destruction by amphipathic alpha-helical antimicrobial peptides. Biochim Biophys Acta 1758(9):1245–1256

Selsted ME, Ouellette AJ (2005) Mammalian defensins in the antimicrobial immune response. Nat Immunol 6(6):551–557

Selsted ME, Novotny MJ, Morris WL, Tang YQ, Smith W, Cullor JS (1992) Indolicidin, a novel bactericidal tridecapeptide amide from neutrophils. J Biol Chem 267(7):4292–4295

Shafer WM, Hubalek F, Huang M, Pohl J (1996) Bactericidal activity of a synthetic peptide (CG 117-136) of human lysosomal cathepsin G is dependent on arginine content. Infect Immun 64(11):4842–4845

Sitaram N, Nagaraj R (1999) Interaction of antimicrobial peptides with biological and model membranes: structural and charge requirements for activity. Biochim Biophys Acta 1462(1–2):29–54

Standley SM, Toft DJ, Cheng H, Soukasene S, Chen J, Raja SM, Band V, Band H, Cryns VL, Stupp SI (2010) Induction of cancer cell death by self-assembling nanostructures incorporating a cytotoxic peptide. Cancer Res 70(8):3020–3026

Strom MB, Haug BE, Skar ML, Stensen W, Stiberg T, Svendsen JS (2003) The pharmacophore of short cationic antibacterial peptides. J Med Chem 46(9):1567–1570

Subbalakshmi C, Sitaram N (1998) Mechanism of antimicrobial action of indolicidin. FEMS Microbiol Lett 160(1):91–96

Subbalakshmi C, Bikshapathy E, Sitaram N, Nagaraj R (2000) Antibacterial and hemolytic activities of single tryptophan analogs of indolicidin. Biochem Biophys Res Commun 274(3):714–716

Tam JP, Lu YA, Yang JL (2002) Antimicrobial dendrimeric peptides. Eur J Biochem 269(3):923–932

Wang H, Xu K, Liu L, Tan JP, Chen Y, Li Y, Fan W, Wei Z, Sheng J, Yang Y–Y (2010) The efficacy of self-assembled cationic antimicrobial peptide nanoparticles against Cryptococcus neoformans for the treatment of meningitis. Biomaterials 31(10):2874–2881

Wang J, Wong ES, Whitley JC, Li J, Stringer JM, Short KR, Renfree MB, Belov K, Cocks BG (2011) Ancient antimicrobial peptides kill antibiotic-resistant pathogens: australian mammals provide new options. PLoS One 6(8):e24030

Wieprecht T, Apostolov O, Beyermann M, Seelig J (1999) Thermodynamics of the alpha-helix-coil transition of amphipathic peptides in a membrane environment: implications for the peptide-membrane binding equilibrium. J Mol Biol 294(3):785–794

Wiradharma N, Khan M, Yong LK, Hauser CAE, Seow SV, Zhang SG, Yang YY (2011a) The effect of thiol functional group incorporation into cationic helical peptides on antimicrobial activities and spectra. Biomaterials 32(34):9100–9108

Wiradharma N, Khoe U, Hauser CA, Seow SV, Zhang S, Yang YY (2011b) Synthetic cationic amphiphilic α-helical peptides as antimicrobial agents. Biomaterials 32(8):2204–2212

Yang L, Harroun TA, Weiss TM, Ding L, Huang HW (2001) Barrel-stave model or toroidal model? A case study on melittin pores. Biophys J 81(3):1475–1485

Yeung AT, Gellatly SL, Hancock RE (2011) Multifunctional cationic host defence peptides and their clinical applications. Cell Mol Life Sci 68(13):2161–2176

Yin LM, Edwards MA, Li J, Yip CM, Deber CM (2012) Roles of hydrophobicity and charge distribution of cationic antimicrobial peptides in peptide-membrane interactions. J Biol Chem 287(10):7738–7745

Yoon WH, Park HD, Lim K, Hwang BD (1996) Effect of O-glycosylated mucin on invasion and metastasis of HM7 human colon cancer cells. Biochem Biophys Res Commun 222(3):694–699

Zasloff M (2002) Antimicrobial peptides of multicellular organisms. Nature 415(6870):389–395. doi:10.1038/415389a

Zelezetsky I, Pag U, Sahl H-G, Tossi A (2005) Tuning the biological properties of amphipathic α-helical antimicrobial peptides: rational use of minimal amino acid substitutions. Peptides 26(12):2368–2376

Zheng L, McQuaw CM, Ewing AG, Winograd N (2007) Sphingomyelin/phosphatidylcholine and cholesterol interactions studied by imaging mass spectrometry. J Am Chem Soc 129(51):15730–15731